magnetochemistry

MDPI

Communication

A New Organic Conductor of Tetramethyltetraselenafulvalene (TMTSF) with a Magnetic Dy(III) Complex

Qingyun Wan [1,2,*], Masanori Wakizaka [1,*], Haitao Zhang [1], Yongbing Shen [3], Nobuto Funakoshi [1], Chi-Ming Che [2], Shinya Takaishi [1,*] and Masahiro Yamashita [1,4,*]

[1] Department of Chemistry, Graduate School of Science, Tohoku University, Aramaki-Aza-Aoba, Aoba-ku, Sendai 980-8578, Japan
[2] Department of Chemistry, State Key Laboratory of Synthetic Chemistry, HKU-CAS Joint Laboratory on New Materials, The University of Hong Kong, Pokfulam Road, Hong Kong, China
[3] Frontier Institute of Science and Technology (FIST), State Key Laboratory for Mechanical Behavior of Materials, MOE Key Laboratory for Nonequilibrium Synthesis of Condensed Matter, Xi'an Jiaotong University, 99 Yanxiang Road, Xi'an 710054, China
[4] School of Materials Science and Engineering, Nankai University, Tianjin 300350, China
* Correspondence: qywan@connect.hku.hk (Q.W.); masanori.wakizaka.a7@tohoku.ac.jp (M.W.); shinya.takaishi.d8@tohoku.ac.jp (S.T.); yamasita@agnus.chem.tohoku.ac.jp (M.Y.); Tel.: +81-22-765-6547 (M.Y.)

Abstract: A new molecular conductor of $(TMTSF)_5[Dy(NCS)_4(NO_3)_2]CHCl_3$ was prepared using the electrochemical oxidation method. The complex crystallizes in the $Cmc2_1$ (36) space group, where the partially-oxidized TMTSF molecules form a 1D (one-dimensional) column structure. The crystal shows a semiconducting behavior with a room temperature conductivity of 0.2 $S{\cdot}cm^{-1}$ and an activation energy of 34 meV at ambient pressure.

Keywords: organic conductor; electro-crystallization; Dysprosium(III); TMTSF

Citation: Wan, Q.; Wakizaka, M.; Zhang, H.; Shen, Y.; Funakoshi, N.; Che, C.-M.; Takaishi, S.; Yamashita, M. A New Organic Conductor of Tetramethyltetraselenafulvalene (TMTSF) with a Magnetic Dy(III) Complex. *Magnetochemistry* **2023**, *9*, 77. https://doi.org/10.3390/magnetochemistry9030077

Academic Editors: Laura C. J. Pereira and Dulce Belo

Received: 8 February 2023
Revised: 25 February 2023
Accepted: 3 March 2023
Published: 6 March 2023

1. Introduction

The TMTSF cation constituted the first organic superconductor of $(TMTSF)_2PF_6$ and was reported in 1980 [1], describing a quasi 1D charge-transfer salt system with a superconducting transition temperature (T_c) of 0.9 K under 12 kbar by the suppression of spin density wave (SDW) state. Since then, over 100 organic superconductors have been reported and studied [2–5]. For example, β'-$(BEDT\text{-}TTF)_2ICl_2$ [BEDT-TTF = bis(ethylenedithio)tetrathiafulvalene] was reported to have a high T_c of 14.2 K under 82 kbar [6], and its superconducting state is obtained under high pressure to suppress the antiferromagnetic Mott insulating state. Other organic conducting systems include potassium-doped para-terphenyl, which shows step-like transitions at about 125 K in the temperature dependent magnetization curve [7].

The search for new organic superconductors and conductors is still ongoing [8–17], and it is interesting to investigate the effects of 4f electrons on the conductivity properties of TMTSF molecules [18,19]. Our group has been working on functional molecular conductors and single-molecule magnets (SMMs) for a long time, reporting various hybrid systems by combining different conductors of TTF (tetrathiafulvalene), BEDT-TTF, $M(dmit)_2$ (dmit = 4,5-dimercapto-1,3-dithiole-2-dithione), and BEDO-TTF (bis(ethylenedioxy)tetrathiafulvalene) with different single-molecule magnets (SMMs) such as $[Co(pdms)_2]^{2-}$, $[Dy(NCS)_7]^{4-}$, $[Mn_2]^{2+}$ clusters, and so on [20–26]. The 4f electrons are well known to have large anisotropic magnetic moments due to strong spin-orbital coupling, which is distinct from 3d electrons. The use of a polyvalent 4f metal complex as a counter-anion also indicates a different degree of conduction band filling in the radical of TMTSF molecules, compared to that of monovalent anions such as PF_6^-, Cl^-, I^-, and so on [2]. Such a change in the filling in the conduction band may lead to new physical properties of the molecular conductors.

Herein, we used a polyvalent 4f metal complex of $[Dy(NCS)_4(NO_3)_2]^{3-}$ as the counter-anion to prepare a new quasi-1D magnetic molecular conductor of $(TMTSF)_5[Dy(NCS)_4(NO_3)_2]CHCl_3$ (**1**, Scheme 1) using an electro-crystallization method. Synthesis, crystal structure, conductivity, optical, magnetic properties, and band structure calculations of **1** have been investigated and discussed in the present work.

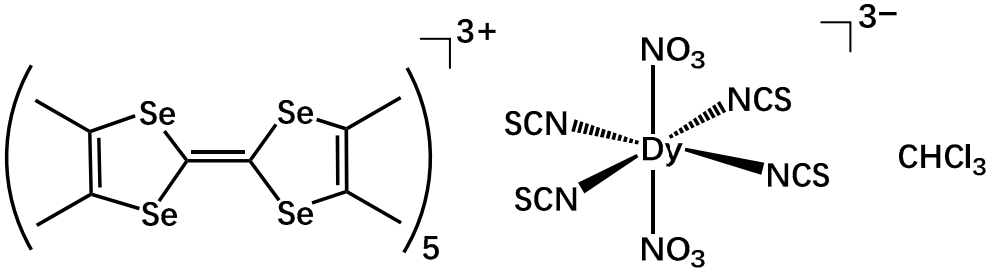

Scheme 1. Chemical structure of compound **1**.

2. Materials and Methods

2.1. Synthesis

TMTSF, $Dy(NO_3)_3{\cdot}6H_2O$, tetrabutylammonium (TBA) thiocyanate salts, and organic solvents were commercially purchased and used without any further purification. $(TBA)_3Dy(NCS)_4(NO_3)_2$ complexes were obtained by following reported procedures [27].

Crystals of **1** were synthesized using an electro-crystallization method of TMTSF (10 mg) and $(TBA)_3Dy(NCS)_4(NO_3)_2$ (80 mg) in $CHCl_3$ (12 mL), with an addition of EtOH (3 mL) on an ITO electrode under galvanostatic conditions (I = 0.5–2 μA) at 25 °C. The crystals of complex **1** grew for 2–4 days depending on the applied current as thin black needles of different sizes.

2.2. Physical Measurements

We measured the temperature-dependent resistivity of compound **1** by using a Quantum Design PPMS 6000 (Quantum Design, San Diego, CA, USA) and Keithley 2611 System Source Meter (Keithley Instruments, Solon, OH, USA). The four-probe method was used, and the measurement was performed under ambient pressure. Gold wires (30 μm diameter) were used to attach the crystal, and carbon paste was used as the electrode.

Single-crystal X-ray crystallographic measurements were performed by using a Rigaku Saturn 70 CCD Diffractometer at 120 K. Graphite-monochromated Mo Kα radiation (λ = 0.71073 Å) was generated by a VariMax microfocus X-ray rotating anode source. We used the CrystalClear crystallographic software package for data processing. The structures were solved and refined by using direct methods included in SIR-92 and SHELXL-2013, respectively [28–30]. The non-H atoms were refined anisotropically, and H atoms were refined by a riding model and were attached to the C atoms using idealized geometries.

We performed the magnetic measurements on compound **1** using MPMS3 (Quantum Design) in the direct current (dc) mode and the alternating current (ac) mode, respectively. We filled the powders sample of compound **1** into a gelatin capsule. Eicosane with a melting point of 310 K was used to fix the sample in a plastic straw.

2.3. Computational Methodology

The band structure of compound **1** was calculated by VASP (Vienna Ab initio Simulation Package) [31,32] using the Perdew-Burke-Ernzerhof (PBE) exchange-correlation functional [33] with a kinetic energy cutoff of 640 eV. PAW pseudopotentials were applied to describe the Dy, Se, C, N, H, O, and Cl atoms [34], where the *f* electrons of Dy are kept frozen in the core and described by the selected pseudopotentials. A 2 × 4 × 2 Monkhorst-Pack k-mesh was employed for the self-consistent calculation to obtain a converged charge density for the further band structure calculation.

To estimate the charge transfer integrals between two TMTSF units, the energy-splitting-in-dimer (ESID) method was applied [35]. The wavefunction of the dimers was obtained using the Gaussian16 program package [36] under a PBE0/def2-TZVP level [37,38]. The tight convergence threshold (10^{-8} for the root mean square change in the density matrix) was used for the SCF procedure.

3. Results and Discussion

3.1. Crystal Structures

Compound (**1**) crystallized in the $Cmc2_1$ (36) space group with five TMTSF units, one $[Dy(NCS)_4(NO_3)_2]^{3-}$ unit, and one $CHCl_3$ molecule. TMTSF molecules form a quasi-1D π-π stacking column structure along the b axis as shown in Figure 1d. We checked the intermolecular π-π distance between neighboring TMTSF molecules in the 1D column. A small difference of intermolecular distance of 3.44(1) Å and 3.50(1) Å has been observed between each TMTSF molecule in the 1D column, suggesting a dimerization process of TMTSF molecules in the 1D column. Among five TMTSF molecules, four out of them (TMTSF-b1 and TMTSF-b2) were located in the 1D column, while one TMTSF (TMTSF-a) shows orthogonal (T-shaped) packing form with the 1D column structure (Figure 1a). The distance between the TMTSF-a and TMTSF-b2 molecules is 3.71 Å, and the close distance indicates a T-type packing interaction between these two molecules (Figure 1c) [39]. Along the c-axis, the layer is constituted by radical cations of TMTSF-a and $[Dy(NCS)_4(NO_3)_2]^{3-}$ units alternatively. A close distance of 4.95 Å between TMTSF-b1 and complex $[Dy(NCS)_4(NO_3)_2]^{3-}$ was observed (Figure 1c). Compound **1** shows rectangular cavities in its crystal structure (Figure 1c) with a size of 15.15 Å × 12.16 Å; they are built up by alternating TMTSF-a and $[Dy(NCS)_4(NO_3)_2]^{3-}$ units, and the cavities are occupied exclusively by TMTSF-b column.

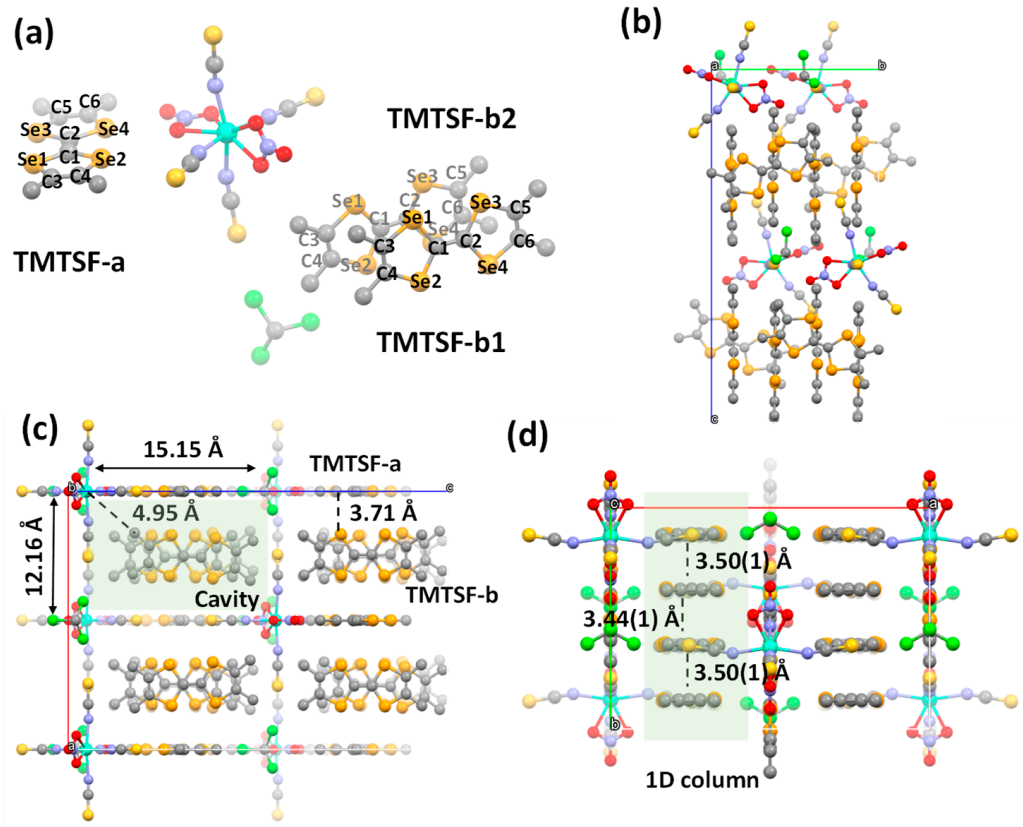

Figure 1. (**a**) X-ray crystal structure of **1**. Crystal packing along the (**b**) a-axis, (**c**) b-axis and (**d**) c-axis.

An examination of intramolecular C-C and C-Se distances in TMTSF-a and TMTSF-b molecules (Figure 1a) was conducted, and the results are summarized in Table 1. A closer C1-C2 is observed in the TMTSF-a molecule (1.31(2) Å) compared to that in TMTSF-b

(1.385(11) and 1.392(10) Å). The different intramolecular bond length indicates a different charge density for TMTSF-a and TMTSF-b molecules in compound **1**. We made a comparison of the C1-C2 distance between TMTSF molecules in compound **1** and other reported TMTSF-type organic conductors, and summarized the results in Table S2. The charge-neutral TMTSF molecule has a C1-C2 distance of 1.347 Å [40]. The TMTSF molecule with an average oxidation ranging from +0.5, to +2/3, to +1 has the C1-C2 distance from 1.430 Å to 1.316 Å [41–47], with no clear relationship between the C1-C2 distance and the charge density of the TMTSF molecule.

Table 1. Intramolecular bond length of TMTSF-a and TMTSF-b molecule in compound **1**.

Bond Length	TMTSF-a	TMTSF-b1	TMTSF-b2
C1-C2	1.31(2) Å	1.385(11) Å	1.392(10) Å
C1-Se1	1.915(13) Å	1.867(7) Å	1.865(7) Å
C1-Se2	1.923(18) Å	1.867(8) Å	1.879(8) Å
C2-Se3	1.917(12) Å	1.885(7) Å	1.871(8) Å
C2-Se4	1.919(19) Å	1.866(8) Å	1.877(7) Å
C3-C4	1.34(3) Å	1.336(13) Å	1.354(12) Å
C5-C6	1.39(2) Å	1.339(13) Å	1.368(13) Å

3.2. Conductivity Properties

Single-crystal temperature-dependent resistivity measurements were performed on compound **1** using the four-probe method along the b-axis of the crystal. The σ-T^{-1} relationship shows a semiconductive behavior in Figure 2a, based on a decreased resistivity upon increasing the temperature. Conductivity of **1** at room temperature (σ_{rt}) was determined to be 0.2 S·cm^{-1}. Analysis of the Ln(σ) versus T^{-1} plot shows a linear curve, as shown in Figure 2b. The curve was fitted using a linear function giving an activation energy (E_a) of 34 meV at ambient pressure, which is the energy difference between the transport level and the Fermi level of compound **1** [48]. The resistivity measurements were performed on another two crystals of compound **1**, giving similar σ_{rt} and E_a values (Figure S1).

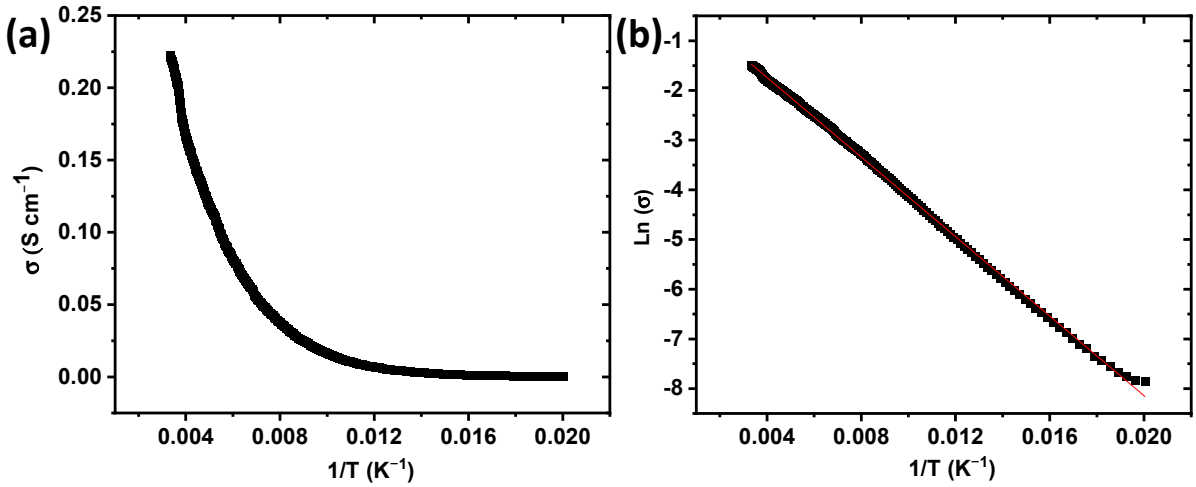

Figure 2. (**a**) Temperature dependence of σ (S·cm^{-1}) for a single crystal of **1**. (**b**) Ln(σ)-T^{-1} and its fitting curve to a linear function (red line).

Since $[Dy(III)(NCS)_4(NO_3)_2]^{3-}$ anion's charge is −3 and the unit cell contains five TMTSF molecules, the valence band made by TMTSF molecules should be partially filling. Such a partially-filled band structure usually leads to metallic behavior instead of semiconductivity [49]. We note that the semiconductive or insulating behavior also shows up in other organic conductors with a partially-filled band, such as $(TMTSF)_2X$ (X = PF_6, AsF_6, SbF_6, TaF_6, NbF_6) where a metal-insulating transitions occurs at 11–17 K [2], and (BEDT-

TTF)$_2$X with a Mott transition near the superconducting state in its phase diagram [3]. The formal oxidation state of TMTSF and BEDT-TTF molecules in these organic conductors is +0.5, indicating a quarter filling of the valence band. The insulating or semiconductive behavior is due to a dimerization of TMTSF or BEDT-TTF molecules, making the charge density +1 per site (Figure 3a). Mott localization occurs subsequently, based on the Coulomb repulsion (***U***) between dimers, leading to an opening of the gap in their band structures (Figure 3c) [3,10]. In compound **1**, a similar dimerization was observed between two TMTSF-b molecules (Figure 1d). We conceive that two possibilities may lead to the non-metallic behaviors of compound **1**: (a) formation of a dimer-Mott state where an overall charge density of +1 may populate over the TMTSF-b dimer and a +1 charge is assigned for the TMTSF-a molecule (Figure 3a), and (b) formation of a charge-ordering state due to the charge disproportion for the TMTSF-b molecules, as shown in Figure 3b. Under these two conditions, the TMTSF-b dimer would form a half-filled band in the 1D column structure. The hopping integral (***t***) would be small due to a relatively long intermolecular distance of 3.50 Å between two TMTSF-b dimers. The Mott insulating phase shows up [3], leading to the semiconductive behavior of compound **1**.

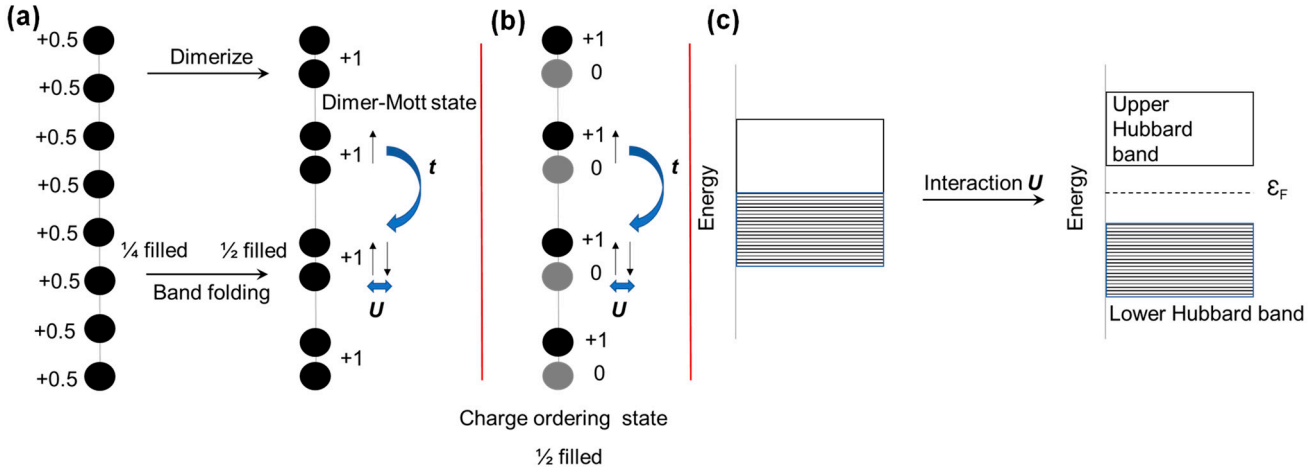

Figure 3. Schematic drawing of possible mechanisms to account for the non-metallic behaviors of compound **1**: the formation of a (**a**) dimer-Mott state, (**b**) a charge-ordering state, or (**c**) formation of upper Hubbard band and lower Hubbard band in the Mott-Hubbard insulators.

A comparison was made among compound **1** and other organic conductors containing 4f metal complexes regarding the conductivity properties. The reported (BEDT-TTF)$_5$[Ln(NCS)]$_6$ (Ln = Ho, Er, Yb and Y) compound has a semiconductive behavior with a large activation energy of ~1.5 eV and the resistivity of 4–6 Ω·cm at 280 K [50]. Two BEDT-TTF molecules co-exist in the crystal structure of (BEDT-TTF)$_5$[Ln(NCS)]$_6$; one is BEDT-TTF$^+$ and the other is BEDT-TTF$^{+0.5}$. The BEDT-TTF$^{+0.5}$ molecule forms a chain structure, and a dimerization of BEDT-TTF molecules leads to Mott localization and the semiconductive behavior of (BEDT-TTF)$_5$[Ln(NCS)]$_6$. The reported (BEDT-TTF)$_5$Dy(NCS)$_7$(KCl)$_{0.5}$ compound has a comparable value of σ_{rt} (1.7 S·cm^{-1}) with compound **1** [20]. (BEDT-TTF)$_5$Dy(NCS)$_6$(NO_3)C_2H_5OH compound is a semiconductor and has a smaller σ_{rt} of 0.01–0.1 S·cm^{-1} and 1–7 × 10^{-5} S·cm^{-1} along two axes of the crystal structure compared to **1** [18]. In the literature, room-temperature conductivities of (BEDT-TTF)$_2$[$HoCl_2$(H_2O)$_6$]Cl_2(H_2O)$_2$, (BEDT-TTF)$_2$Ln'Cl_4(H_2O)$_n$(Ln' = Dy, Tb, Ho) crystals were measured and determined to be 0.004, 0.007, 0.0008, and 0.035 S/cm, respectively, with semiconductor behavior and an activation energy of conductivity of 220 meV, 300 meV, 320, and 290 meV, respectively [51]. Several factors can influence the conductivity properties of molecular conductors, including the degree of charge transfer, dimensionality, and conformation variations in the radical cations [3,18]. Moreover, these factors are considered to lead to the discrepancy of conductivity properties among these 4f-π organic conductors. A high degree

of charge-transfer interaction and high dimensionality usually leads to high conductivity and superconductivity behaviors [3,22].

3.3. Optical Properties

To further investigate the electronic structure of **1**, a polarized IR (infrared) reflectance spectrum was recorded for the crystal of **1**. The excitation light was polarized along (// direction) and perpendicular (⊥ direction) to the long axis of the crystal, respectively. As shown in Figure 4, the intensity of the reflection spectrum recorded at the // direction is stronger than that along the ⊥ direction, indicating an anisotropic 1D electronic structure of compound **1**. A broad peak around 100 meV was observed in the reflectance spectrum, which is attributed to the existence of a small energy band gap of crystal **1** in its band structure.

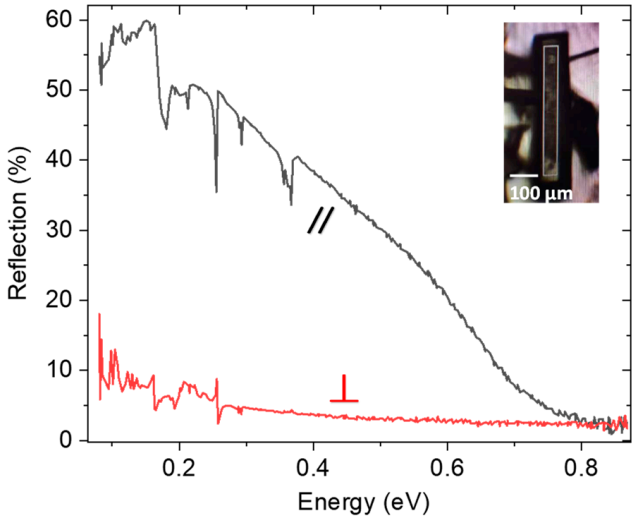

Figure 4. Polarized IR reflectance spectrum of crystal **1** at room temperature. Inset is the optical image of the crystal. Black line: excitation along the direction of the crystal. Red line: excitation perpendicular to the direction of the crystal.

3.4. Magnetic Properties

The magnetic field dependence of static normalized magnetization (M/M_s) was measured on polycrystalline samples of **1** at 1.8 K (Figure 5). The magnetization process is considered to be mostly contributed by a Dy(III) complex having a large magnetic moment (J = 15/2, S = 5/2, L = 5), with minor contributions from the TMTSF radical cations. No hysteresis was observed for compound **1** at 1.8 K (Figure 5a). The temperature dependence of the magnetization curves was simulated on the PHI program using the following spin Hamiltonian (Figure 5b) [52]:

$$\hat{\mathcal{H}}_{SO} = \lambda \hat{\boldsymbol{L}} \cdot \hat{\boldsymbol{S}} \quad (1)$$

$$\hat{\mathcal{H}}_{ZEE} = \mu_B \hat{\boldsymbol{S}} \cdot g_J \cdot \hat{\boldsymbol{B}} \quad (2)$$

$$\hat{\mathcal{H}}_{ZFS} = D\left\{\hat{S}_z^2 - \frac{1}{3}S(S+1)\right\} \quad (3)$$

where λ, $\boldsymbol{L}$, $\boldsymbol{S}$, and $\boldsymbol{B}$ with hats, μ_B, g_J, D, and S refer to spin–orbit coupling constant, operators of orbit and spin, magnetic field, the Bohr magneton, g-factor for lanthanide, axial zero-field splitting (ZFS) constant, and total spin on the metal ion, respectively. The simulation curves were applied typical values of g_J = 4/3 and $\lambda = -360$ cm^{-1} [52,53]. Without the ZFS parameter, the simulation curves (dotted lines) do not match with the experiment plots. In contrast, applying $D = -0.9$ cm^{-1} matches well with the experimental plots, suggesting that Dy(III) centers in **1** have a small negative D term. A negative D term is necessary for SMMs with uniaxial anisotropy. However, D of -0.9 cm^{-1} is

too small to induce hysteresis. As expected, the dynamic susceptibility exhibited no significant signals at 1.8 K in the measurement range in Figure S2. The susceptibility of the out-of-phase component (χ'') rises at a higher frequency region in Figure S2, suggesting that the peak would be out of measurement range (>1000 Hz) and a very fast magnetic relaxation of SMMs of compound **1**. Among the reported 4f-π system, SMM behavior was observed in the $(BEDT\text{-}TTF)_5Dy(NCS)_7(KCl)_{0.5}$ system [20], while it is absent in $(BEDT\text{-}TTF)_2[HoCl_2(H_2O)_6]Cl_2(H_2O)_2$ and $(BEDT\text{-}TTF)_2Ln'Cl_4(H_2O)_n$(Ln' = Dy, Tb, Ho) compounds [51]. Molecular symmetry is found to be closely related to SMM properties [54], and is considered to be a probable reason for the existence of strong and weak SMM properties in $(BEDT\text{-}TTF)_5Dy(NCS)_7(KCl)_{0.5}$ and compound **1**, respectively, as well as the absence of SMM properties in $(BEDT\text{-}TTF)_2[HoCl_2(H_2O)_6]Cl_2(H_2O)_2$ and $(BEDT\text{-}TTF)_2Ln'Cl_4(H_2O)_n$ compounds.

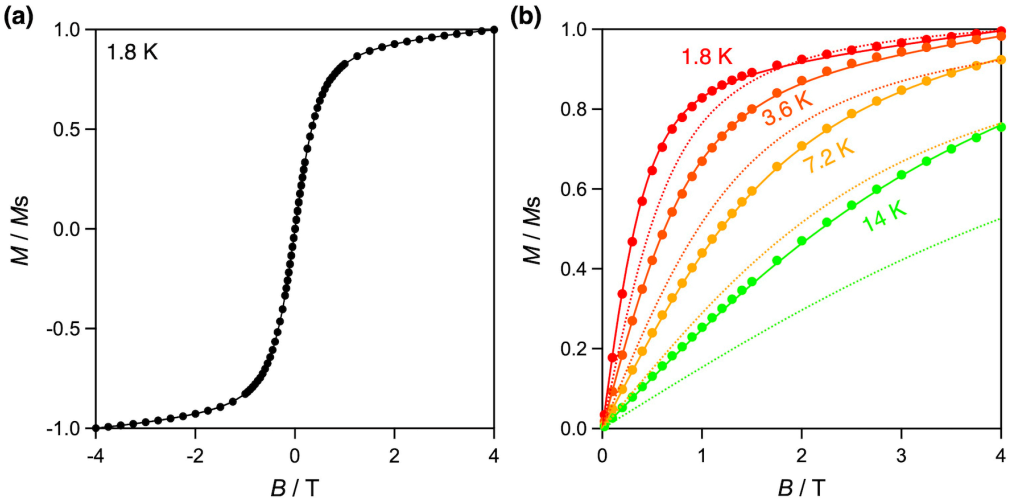

Figure 5. Magnetic field-dependent magnetization of compound **1**. (**a**) Loop at 1.8 K and (**b**) curves at 1.8 K (red line), 3.6 K (orange line), 7.2 K (yellow line), and 14 K (lime-green line). The solid-colored lines show the simulation curves using $S = 5/2$, $L = 5$, $g_J = 4/3$, $\lambda = -360$ cm^{-1}, $D = -0.9$ cm^{-1}, whereas the dotted lines are fitting curves without the D term.

We further examined the magnetoresistance (MR) of compound **1** and the results are shown in Figure 6. Negative MR was observed for compound **1**, where the MR approaches −3.5% under a magnetic field of 9 T at 30 K.

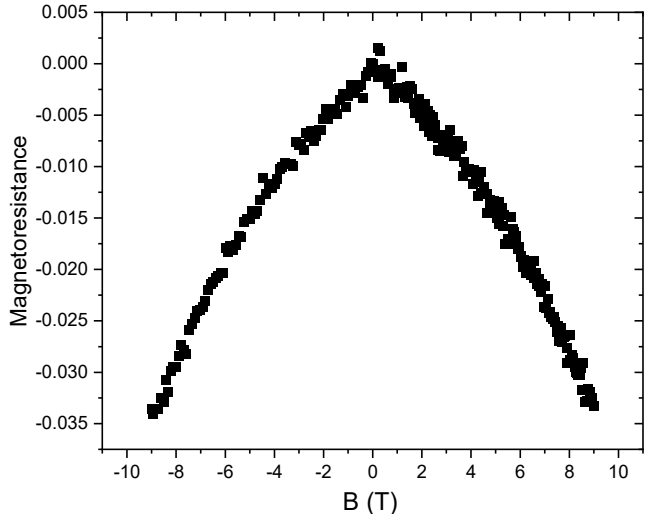

Figure 6. Magnetoresistance of compound **1** under a sweet rate of 20 Oe s^{-1} at the temperature of 30 K.

3.5. Band Structure Calculations

To understand the high conductivity of compound **1** (0.2 S·cm^{-1}), we calculated its band structure, which was shown in Figure 7. The Fermi level was calculated to be at ~1.47 eV which crosses the bands at XS, YG, UR, and TZ directions. The band dispersion is much more significant along the *b* direction compared to that of other two directions, which indicates that the TMTSF units have a stronger orbital overlap along the *b* axis than the other two directions. The partially-filled bands are consistent with the fact that TMTSF molecules in compound **1** are partially oxidized. Notably, the PBE functional lacks accuracy to describe a localized electronic structure; hence, the on-site Coulomb repulsion calculations have not been involved and considered here to describe the Mott-insulating characteristics of compound **1**. We further calculated the charge transfer integral (*t*) between the TMTSF dimer of compound **1** and summarized the results in Figure S3. Larger *t* was calculated and observed for TMTSF-b molecules along the 1D column *b* direction, compared to that of TMTSF-a molecules, indicating the anisotropic 1D nature of the crystal **1**.

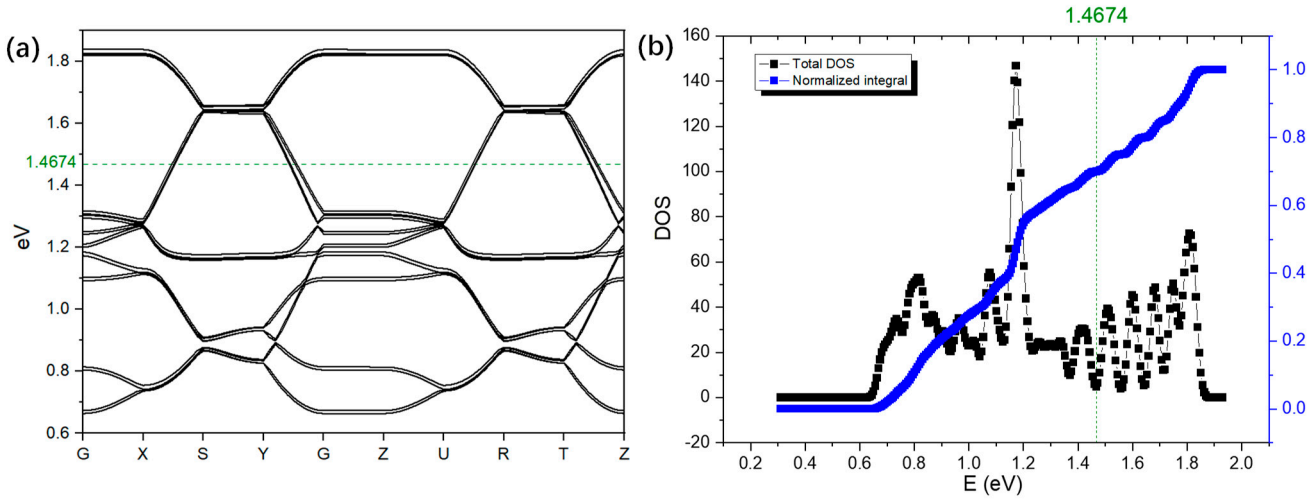

Figure 7. (**a**) The band structure of compound **1**. The corresponding Fermi level is represented by the green dash line. G (0, 0, 0); X (0.5, 0, 0); Y (0, 0.5, 0); Z (0, 0, 0.5); S (0.5, 0.5, 0); U (0.5, 0, 0.5); T (0, 0.5, 0.5); R (0.5, 0.5, 0.5). (**b**) Density of states (DOS) of compound **1**.

4. Conclusions

A new organic conductor (**1**) composed of a 1D cationic TMTSF column and 4f metal complexes of $[Dy(III)(NCS)_4(NO_3)_2]^{3-}$ has been prepared. Its conductivity at room temperature was determined to be 0.2 S·cm^{-1} with an activation energy of 34 meV. This preliminary study provides information for designing new hybrid materials based on molecular conductors and polyvalent magnetic 4f metal complexes.

Supplementary Materials: The following supporting information can be downloaded at: https://www.mdpi.com/article/10.3390/magnetochemistry9030077/s1, Figure S1: (a and c) Temperature dependence of σ (S·cm^{-1}) for two single crystals of **1**. (b and d) Ln(σ)-T^{-1} and its fitting curve to a linear function (red line) of panel a and c, respectively; Figure S2: Frequency dependence of (a) the in-phase and (b) the out-of-phase magnetic susceptibility at 1.8 K as a function of the magnetic field of compound **1**; Figure S3: Calculation of charge transfer integral of *t(hole)* and *t(electron)* in the TMTSF dimers of compound **1**; Table S1: Summary of the crystal data of compound **1**; Table S2: A summary of C1-C2 distance in TMTSF-type molecules.

Author Contributions: M.Y. conceived and designed the experiments; M.W., Q.W. and S.T. performed the experiments; H.Z. performed the calculations; M.W., Q.W., M.Y., N.F., Y.S., S.T. and C.-M.C. analyzed the data; Q.W. wrote the paper. All authors have read and agreed to the published version of the manuscript.

Funding: This work was supported by the JSPS KAKENHI Grant Number JP19H05631 and the National Natural Science Foundation of China (NSFC, 22150710513). M.Y. Thanks the 111 projects (B18030) from China.

Acknowledgments: Thanks all the projects from China and Japan.

Conflicts of Interest: The authors declare no conflict of interest.

References

1. Jérome, D.; Mazaud, A.; Ribault, M.; Bechgaard, K. Superconductivity in a synthetic organic conductor $(TMTSF)_2PF_6$. *J. Phys. Lett.* **1980**, *41*, 95–98. [CrossRef]
2. Mori, H. Materials viewpoint of organic superconductors. *J. Phys. Soc. Jpn.* **2006**, *75*, 051003. [CrossRef]
3. Ardavan, A.; Brown, S.; Kagoshima, S.; Kanoda, K.; Kuroki, K.; Mori, H.; Ogata, M.; Uji, S.; Wosnitza, J. Recent topics of organic superconductors. *J. Phys. Soc. Jpn.* **2011**, *81*, 011004. [CrossRef]
4. Williams, J.M.; Schultz, A.J.; Geiser, U.; Carlson, K.D.; Kini, A.M.; Wang, H.G.; Kwok, W.-K.; Whangbo, M.-H.; Schirber, J.E. Organic superconductors—New benchmarks. *Science* **1991**, *252*, 1501–1508. [CrossRef]
5. Enoki, T.; Miyazaki, A. Magnetic TTF-based charge-transfer complexes. *Chem. Rev.* **2004**, *104*, 5449–5478. [CrossRef]
6. Taniguchi, H.; Miyashita, M.; Uchiyama, K.; Satoh, K.; Môri, N.; Okamoto, H.; Miyagawa, K.; Kanoda, K.; Hedo, M.; Uwatoko, Y. Superconductivity at 14.2 K in layered organics under extreme pressure. *J. Phys. Soc. Jpn.* **2003**, *72*, 468–471. [CrossRef]
7. Liu, W.; Lin, H.; Kang, R.; Zhu, X.; Zhang, Y.; Zheng, S.; Wen, H.-H. Magnetization of potassium-doped p-terphenyl and p-quaterphenyl by high-pressure synthesis. *Phys. Rev. B* **2017**, *96*, 224501. [CrossRef]
8. Kobayashi, H.; Kobayashi, A.; Cassoux, P. BETS as a source of molecular magnetic superconductors (BETS = bis (ethylenedithio) tetraselenafulvalene). *Chem. Soc. Rev.* **2000**, *29*, 325–333. [CrossRef]
9. Enomoto, M.; Miyazaki, A.; Enoki, T. Magnetic Properties of (C1TEX-TTF) $FeBr_4$ (X=S, Se). *Mol. Cryst. Liq. Cryst. Sci. Technol. Sect. A Mol. Cryst. Liq. Cryst.* **1999**, *335*, 293–302. [CrossRef]
10. Anderson, P.; Lee, P.; Saitoh, M. Remarks on giant conductivity in TTF-TCNQ. *Solid State Commun.* **1973**, *13*, 595–598. [CrossRef]
11. Cui, H.; Otsuka, T.; Kobayashi, A.; Takeda, N.; Ishikawa, M.; Misaki, Y.; Kobayashi, H. Structural, electrical, and magnetic properties of a series of molecular conductors based on BDT-TTP and lanthanoid nitrate complex anions (BDT-TTP = 2, 5-bis (1,3-dithiol-2-ylidene)-1,3,4,6-tetrathiapentalene). *Inorg. Chem.* **2003**, *42*, 6114–6122. [CrossRef]
12. Kushch, N.; Bardin, A.; Buravov, L.; Glushakova, N.; Shilov, G.; Dmitriev, A.; Morgunov, R.; Kulikov, A. Synthesis particularities, structure and properties of the radical cation salts ω-$(BEDT\text{-}TTF)_5M(SCN)_6\cdot C_2H_5OH$, M=Mn, Ni. *Synth. Met.* **2014**, *195*, 75–82. [CrossRef]
13. Kushch, N.D.; Buravov, L.I.; Kushch, P.P.; Shilov, G.V.; Yamochi, H.; Ishikawa, M.; Otsuka, A.; Shakin, A.A.; Maximova, O.V.; Volkova, O.S. Multifunctional compound combining conductivity and single-molecule magnetism in the same temperature range. *Inorg. Chem.* **2018**, *57*, 2386–2389. [CrossRef] [PubMed]
14. Zhang, X.; Xie, H.; Ballesteros-Rivas, M.; Woods, T.J.; Dunbar, K.R. Conducting Molecular Nanomagnet of DyIII with Partially Charged TCNQ Radicals. *Chem.–A Eur. J.* **2017**, *23*, 7448–7452. [CrossRef] [PubMed]
15. Sato, T.; Breedlove, B.K.; Yamashita, M.; Katoh, K. Electro-Conductive Single-Molecule Magnet Composed of a Dysprosium (III)-Phthalocyaninato Double-Decker Complex with Magnetoresistance. *Angew. Chem. Int. Ed.* **2021**, *60*, 21179–21183. [CrossRef]
16. Mroweh, N.; Mézière, C.; Pop, F.; Auban-Senzier, P.; Alemany, P.; Canadell, E.; Avarvari, N. In Search of Chiral Molecular Superconductors: κ-$[(S, S)\text{-}DM\text{-}BEDT\text{-}TTF]_2ClO_4$ Revisited. *Adv. Mater.* **2020**, *32*, 2002811. [CrossRef]
17. Pop, F.; Auban-Senzier, P.; Canadell, E.; Avarvari, N. Anion size control of the packing in the metallic versus semiconducting chiral radical cation salts $(DM\text{-}EDT\text{-}TTF)_2XF_6$ (X=P, As, Sb). *Chem. Commun.* **2016**, *52*, 12438–12441. [CrossRef]
18. Kushch, N.; Kazheva, O.; Gritsenko, V.; Buravov, L.; Van, K.; Dyachenko, O. Novel packing type of ET radical cation layers in a new organic conductor $(ET)_5[Dy(NCS)_6NO_3]\cdot C_2H_5OH$ with a metal-complex lanthanide anion. *Synth. Met.* **2001**, *123*, 171–177. [CrossRef]
19. Shvachko, Y.N.; Starichenko, D.; Korolyov, A.; Kushch, N. Temperature evolution of $BEDT\text{-}TTF^{+1/2}$ and Dy^{3+} spin systems in novel organic conductor $(BEDT\text{-}TTF)_2Dy(NO_3)_4$: EPR and SQUID studies. *Synth. Met.* **2008**, *158*, 315–319. [CrossRef]
20. Shen, Y.; Cosquer, G.; Zhang, H.; Breedlove, B.K.; Cui, M.; Yamashita, M. 4f-π Molecular Hybrid Exhibiting Rich Conductive Phases and Slow Relaxation of Magnetization. *J. Am. Chem. Soc.* **2021**, *143*, 9543–9550. [CrossRef]
21. Shen, Y.; Ito, H.; Zhang, H.; Yamochi, H.; Cosquer, G.; Herrmann, C.; Ina, T.; Yoshina, S.K.; Breedlove, B.K.; Otsuka, A. Emergence of metallic conduction and cobalt (II)-based single-molecule magnetism in the same temperature range. *J. Am. Chem. Soc.* **2021**, *143*, 4891–4895. [CrossRef]
22. Shen, Y.; Cosquer, G.; Ito, H.; Izuogu, D.C.; Thom, A.J.; Ina, T.; Uruga, T.; Yoshida, T.; Takaishi, S.; Breedlove, B.K. An Organic-Inorganic Hybrid Exhibiting Electrical Conduction and Single-Ion Magnetism. *Angew. Chem.* **2020**, *132*, 2420–2427. [CrossRef]
23. Hiraga, H.; Miyasaka, H.; Nakata, K.; Kajiwara, T.; Takaishi, S.; Oshima, Y.; Nojiri, H.; Yamashita, M. Hybrid molecular material exhibiting single-molecule magnet behavior and molecular conductivity. *Inorg. Chem.* **2007**, *46*, 9661–9671. [CrossRef]
24. Hiraga, H.; Miyasaka, H.; Takaishi, S.; Kajiwara, T.; Yamashita, M. Hybridized complexes of [MnIII2] single-molecule magnets and Ni dithiolate complexes. *Inorg. Chim. Acta* **2008**, *361*, 3863–3872. [CrossRef]

25. Cosquer, G.; Shen, Y.; Almeida, M.; Yamashita, M. Conducting single-molecule magnet materials. *Dalton Trans.* **2018**, *47*, 7616–7627. [CrossRef] [PubMed]
26. Yamashita, M. Next generation multifunctional nano-science of advanced metal complexes with quantum effect and nonlinearity. *Bull. Chem. Soc. Jpn.* **2021**, *94*, 209–264. [CrossRef]
27. Mullica, D.F.; Bonilla, B.M.; David, M.a.C.; Farmer, J.M.; Kautz, J.A. Synthesis, characterization, and structural analyses of three high-coordination tetra-n-butylammonium lanthanide (III) complexes. *Inorg. Chim. Acta* **1999**, *292*, 137–143. [CrossRef]
28. Altomare, A.; Burla, M.C.; Camalli, M.; Cascarano, G.L.; Giacovazzo, C.; Guagliardi, A.; Moliterni, A.G.; Polidori, G.; Spagna, R. SIR97: A new tool for crystal structure determination and refinement. *J. Appl. Crystallogr.* **1999**, *32*, 115–119. [CrossRef]
29. Farrugia, L.J. WinGX and ORTEP for Windows: An update. *J. Appl. Crystallogr.* **2012**, *45*, 849–854. [CrossRef]
30. Sheldrick, G.M. Crystal structure refinement with SHELXL. *Acta Crystallogr. Sect. C Struct. Chem.* **2015**, *71*, 3–8. [CrossRef]
31. Kresse, G.; Furthmüller, J. Efficiency of ab-initio total energy calculations for metals and semiconductors using a plane-wave basis set. *Comput. Mater. Sci.* **1996**, *6*, 15–50. [CrossRef]
32. Kresse, G.; Furthmüller, J. Efficient iterative schemes for ab initio total-energy calculations using a plane-wave basis set. *Phys. Rev. B* **1996**, *54*, 11169. [CrossRef] [PubMed]
33. Perdew, J.P.; Burke, K.; Ernzerhof, M. Generalized gradient approximation made simple. *Phys. Rev. Lett.* **1996**, *77*, 3865. [CrossRef] [PubMed]
34. Kresse, G.; Joubert, D. From ultrasoft pseudopotentials to the projector augmented-wave method. *Phys. Rev. B* **1999**, *59*, 1758. [CrossRef]
35. Valeev, E.F.; Coropceanu, V.; da Silva Filho, D.A.; Salman, S.; Brédas, J.-L. Effect of electronic polarization on charge-transport parameters in molecular organic semiconductors. *J. Am. Chem. Soc.* **2006**, *128*, 9882–9886. [CrossRef]
36. Frisch, M.; Trucks, G.; Schlegel, H.; Scuseria, G.; Robb, M.; Cheeseman, J.; Scalmani, G.; Barone, V.; Mennucci, B.; Petersson, G. *G09*; Revison D. 01; Gaussian Inc.: Wallingford, CT, USA, 2010.
37. Adamo, C.; Barone, V. Toward reliable density functional methods without adjustable parameters: The PBE0 model. *J. Chem. Phys.* **1999**, *110*, 6158–6170. [CrossRef]
38. Weigend, F.; Ahlrichs, R. Balanced basis sets of split valence, triple zeta valence and quadruple zeta valence quality for H to Rn: Design and assessment of accuracy. *Phys. Chem. Chem. Phys.* **2005**, *7*, 3297–3305. [CrossRef]
39. Grimme, S. Do special noncovalent π–π stacking interactions really exist? *Angew. Chem. Int. Ed.* **2008**, *47*, 3430–3434. [CrossRef]
40. Rani, P.; Rajput, G.; Srivastava, M.; Yadav, R. Structural and vibrational characteristics and vibronic coupling of tetramethyltetraselenafulvalene. *J. Mol. Struct.* **2019**, *1175*, 1–12. [CrossRef]
41. Wu, L.; Coppens, P.; Bu, X. Crystal structure of tetramethyltetraselenafulvalene nitrate,$(C_{10}H_{12}Se_4)NO_3$. *Z. Krist.-New Cryst. Struct.* **1997**, *212*, 101–102. [CrossRef]
42. Rosokha, S.V.; Stern, C.L.; Ritzert, J.T. π-Bonded molecular wires: Self-assembly of mixed-valence cation-radical stacks within the nanochannels formed by inert tetrakis [3,5-bis (trifluoromethyl) phenyl] borate anions. *CrystEngComm* **2013**, *15*, 10638–10647. [CrossRef]
43. Sakata, M.; Yoshida, Y.; Maesato, M.; Saito, G.; Matsumoto, K.; Hagiwara, R. Preparation of superconducting $(TMTSF)_2NbF_6$ by electrooxidation of TMTSF using ionic liquid as electrolyte. *Mol. Cryst. Liq. Cryst.* **2006**, *452*, 103–112. [CrossRef]
44. Wudl, F. Three-dimensional structure of the superconductor $(TMTSF)_2AsF_6$ and the spin-charge separation hypothesis. *J. Am. Chem. Soc.* **1981**, *103*, 7064–7069. [CrossRef]
45. Beno, M.; Blackman, G.; Williams, J.M.; Bechgaard, K. Synthetic metals based on tetramethyltetraselenafulvalene (TMTSF): Synthesis, structure (T = 298 and 125 K), and novel properties of $(TMTSF)_2H_2F_3$. *Inorg. Chem.* **1982**, *21*, 3860–3862. [CrossRef]
46. Emge, T.J.; Beno, M.A.; Daws, C.A.; Wang, H.H.; Williams, J.M. Novel Structural Features, and their Relationship to the Electrical Properties, of the Organic Conductor $(TMTSF)_2NO_3$ at 298 K and 125 K. *Mol. Cryst. Liq. Cryst.* **1984**, *116*, 153–171. [CrossRef]
47. Kazheva, O.N.; Kushch, N.D.; Dyachenko, O.A.; Canadell, E. Rare-earth elements in molecular conductors: Crystal and electronic structures. *J. Solid State Chem.* **2002**, *168*, 457–463. [CrossRef]
48. Mao, L.-F.; Ning, H.; Hu, C.; Lu, Z.; Wang, G. Physical modeling of activation energy in organic semiconductor devices based on energy and momentum conservations. *Sci. Rep.* **2016**, *6*, 24777. [CrossRef] [PubMed]
49. Friedel, J.; Jérome, D. Organic superconductors: The $(TMTSF)_2X$ family. *Contemp. Phys.* **1982**, *23*, 583–624. [CrossRef]
50. Tamura, M.; Matsuzaki, F.; Nishio, Y.; Kajita, K.; Kitazawa, T.; Mori, H.; Tanaka, S. Novel BEDT-TTF salts containing rare earth ions, $(ET)_4Ln(NCS)_6 \cdot CH_2Cl_2$. *Synth. Met.* **1999**, *102*, 1716–1717. [CrossRef]
51. Flakina, A.M.; Zhilyaeva, E.I.; Shilov, G.V.; Faraonov, M.A.; Torunova, S.A.; Konarev, D.V. Layered Organic Conductors Based on BEDT-TTF and Ho, Dy, Tb Chlorides. *Magnetochemistry* **2022**, *8*, 142. [CrossRef]
52. Chilton, N.F.; Anderson, R.P.; Turner, L.D.; Soncini, A.; Murray, K.S. PHI: A powerful new program for the analysis of anisotropic monomeric and exchange-coupled polynuclear d- and f-block complexes. *J. Comput. Chem.* **2013**, *34*, 1164–1175. [CrossRef] [PubMed]

53. Feltham, H.L.; Brooker, S. Review of purely 4f and mixed-metal nd-4f single-molecule magnets containing only one lanthanide ion. *Coord. Chem. Rev.* **2014**, *276*, 1–33. [CrossRef]
54. Liu, J.-L.; Chen, Y.-C.; Tong, M.-L. Symmetry strategies for high performance lanthanide-based single-molecule magnets. *Chem. Soc. Rev.* **2018**, *47*, 2431–2453. [CrossRef] [PubMed]